

Supplementary Materials

From molecular geometry to combustion kinetic model application: ab initio calculations of reaction kinetics between diethyl ether radical and O₂

Hao-Ting Guo^a, Lijun Yang^b, Zeynep Serinyel^c, Chong-
Wen Zhou^{a,d,*}

^a*School of Energy and Power Engineering, Beihang University, Beijing 100191*

^b*School of Astronautics, Beihang University, Beijing 100191*

^c*Institut de Combustion, Aérothermique, Réactivité et Environnement (ICARE), CNRS, Orléans,
France*

^d*Combustion Chemistry Centre, School of Biological and Chemical Sciences, MaREI, Ryan Institute,
University of Galway, Galway H91TK33, Ireland*

E-mail address: chongwen.zhou@universityofgalway.ie (C.-W. Zhou)

When calculating the single-point energies using the QCISD(T) method, care should be taken to observe the T1 diagnostic values to measure the multi-reference state effect. Table S1–S2 presents the T1 diagnostic values for all the species and reaction transition states examined in this paper, with all T1 diagnostic values being less than 0.02 and 0.04 (in some cases < 0.045 [1] may be acceptable) for closed shell and radical species, respectively. The results suggest that the single-reference method can be adequately described for the title system.

Table S1

Species list with their chemical structure and T1 diagnostic values

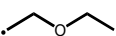
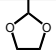
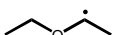
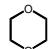
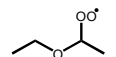
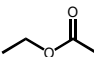
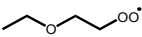
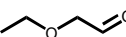
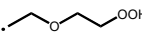
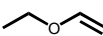
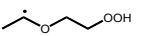
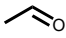

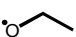
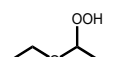
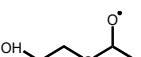
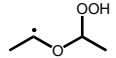
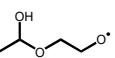
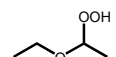
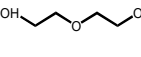
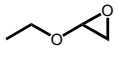
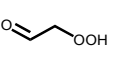
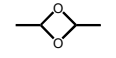
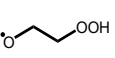
Species	Structure	T1 diagnostic	Species	Structure	T1 diagnostic
C ₂ H ₅ OC ₂ H ₄ -1		0.010	CCY(COCCO)		0.011
C ₂ H ₅ OC ₂ H ₄ -2		0.015	CY(CCOCCO)		0.011
C ₂ OC ₂ -2OO		0.026	C ₂ OC(=O)CH ₃		0.013
C ₂ OC ₂ -1OO		0.025	C ₂ OCC=O		0.013
C ₂ OC ₂ -1O ₂ H-B		0.011	C ₂ OC ₂ H ₃		0.012
C ₂ OC ₂ -1O ₂ H-A		0.014	CH ₃ CHO		0.015
C ₂ OC ₂ -1O ₂ H-2		0.016	C ₂ H ₅ O		0.023
C ₂ OC ₂ -2O ₂ H-1		0.014	HOC ₂ OC ₂ -2O		0.018
C ₂ OC ₂ -2O ₂ H-A		0.014	CC(OH)OCC-1O		0.016
C ₂ OC ₂ -2O ₂ H-B		0.011	HOC ₂ OC ₂ -1O		0.015
C ₂ OCY(COC)		0.011	O=CCOOH		0.014
CCY(COCO)C		0.011	OCCOOH		0.016

Table S2

T1 diagnostic values for the reaction transition states involved in this study

Reaction Channel	T1 diagnostic	Reaction Channel	T1 diagnostic
W1 \rightleftharpoons W2	0.032	W5 \rightleftharpoons P3	0.029
W1 \rightleftharpoons W3	0.026	W6 \rightleftharpoons P9	0.035
W1 \rightleftharpoons W4	0.025	W6 \rightleftharpoons P2	0.038
W1 \rightleftharpoons P1	0.027	W6 \rightleftharpoons P3	0.028
W1 \rightleftharpoons P3	0.029	W6 \rightleftharpoons P10	0.026
W2 \rightleftharpoons P2	0.031	W7 \rightleftharpoons P6	0.036
W2 \rightleftharpoons W3	0.013	W7 \rightleftharpoons P11	0.039
W2 \rightleftharpoons P3	0.035	W7 \rightleftharpoons P8	0.015
W3 \rightleftharpoons P4	0.032	W7 \rightleftharpoons P9	0.013
W3 \rightleftharpoons P5	0.031	W8 \rightleftharpoons P12	0.023
W4 \rightleftharpoons P1	0.019	W8 \rightleftharpoons P9	0.014
W4 \rightleftharpoons P6	0.03	W8 \rightleftharpoons P13	0.020
W4 \rightleftharpoons P7	0.036	W8 \rightleftharpoons P14	0.030
W4 \rightleftharpoons P8	0.03	R1 \rightleftharpoons R2	0.014
W5 \rightleftharpoons W6	0.032	R1 \rightleftharpoons P15	0.027
W5 \rightleftharpoons W7	0.026	R1 \rightleftharpoons P17	0.015
W5 \rightleftharpoons W8	0.025	R2 \rightleftharpoons P16	0.031
W5 \rightleftharpoons P9	0.027	R2 \rightleftharpoons P17	0.018

The active space (7e,5o) was chosen for the calculation of 1-ethoxyethyl radical + O₂. The orbital shapes and electron occupation numbers calculated using CASPT2(7e,5o)/cc-pVDZ for the geometry with a C-O radical separation of 2 Å were listed in Table S3. Figure S1 presents the interaction potential energy surfaces and 1-D total energy corrections for the barrierless channel of $\dot{\text{C}}\text{H}_2\text{CH}_2\text{OC}_2\text{H}_5 + \text{O}_2$ along with the C-O bond ranging over 1.8–10 Å. The interaction energies at rigid geometry exhibit relatively higher values at C-O distances ranging from 1.8 to 3 Å. In contrast, calculations employing with high-level basis set in relaxed geometry show lower potential energies. The relaxation geometry correction has a major effect on the interaction potential between the two fragments at C-O distance less than 3 Å, ranging from -5.91 kcal mol⁻¹ at 1.8 Å to -0.04 kcal mol⁻¹ at 3 Å. Meanwhile, the basis set energy correction ranges from -2.21 kcal mol⁻¹ at 1.8 Å to 0.16 kcal mol⁻¹ at 3 Å. When C-O distance is larger than 3 Å, the geometry and basis set corrections are close to each other and their effect on the interaction energies between the two fragments are small.

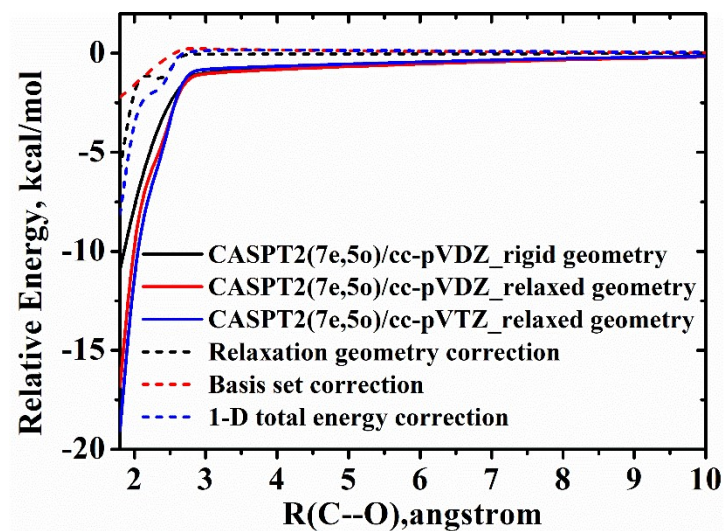


Figure S1. Potential energy surfaces including relaxation geometry correction and basis set correction for 1-ethoxyethyl radical + O₂

Table S3. The orbitals and electron occupations obtained at the CASPT2(7e,5o)/cc-pVDZ level of theory for C–O distances at 2 Å.

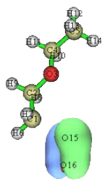
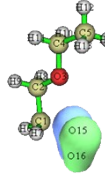
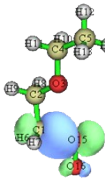
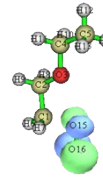
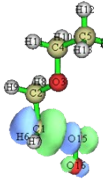
Orbital shape					
	O lone pair	O15-O16 π bond	O15-C1 σ bond	O15-O16 π^* bond	O15-C1 σ^* bond
Orbital number	26	27	28	29	30
Electron occupation number	1.9594	1.9582	1.7168	1.0406	0.3247
Orbital Energy/eV	-18.16	-17.76	-8.10	-5.04	1.49

Table S4

The relative energies at QCISD(T)/CBS//M06-2X/6-311++G(d,p), M06-2X/6-311++G(d,p) and relative enthalpies at 298 K, with R1 + ³O₂ as the zero point energy, in kcal mol⁻¹.

Species	Relative energy at QCISD(T)/CBS//M06- 2X/6-311++G(d,p)	Relative energy at M06- 2X/6-311++G(d,p)	Relative enthalpy ($\Delta H_{f,298K}$)
R1 + $^3\text{O}_2$	0	0	0
W1	-36.01	-35.69	-37.53
W2	-18.41	-16.59	-18.09
W3	-25.91	-23.13	-25.66
W4	-19.39	-17.43	-19.37
P1	-79.83	-79.37	-80.55
P2	-33.16	-33.52	-33.66
P3	-12.04	-8.52	-11.12
P4	-55.72	-51.26	-53.18
P5	-49.96	-48.47	-50.0
P6	-57.61	-56.36	-57.85
P7	-70.96	-70.42	-71.1
P8	-7.05	-2.14	-6.58

Table S5

The relative energies at QCISD(T)/CBS//M06-2X/6-311++G(d,p), M06-2X/6-311++G(d,p) and relative enthalpies at 298 K, with R2 + $^3\text{O}_2$ as the zero point energy, in kcal mol⁻¹.

Species	Relative energy at QCISD(T)/CBS//M06- 2X/6-311++G(d,p)	Relative energy at M06- 2X/6-311++G(d,p)	Relative enthalpy ($\Delta H_{f,298K}$)
R2 + $^3\text{O}_2$	0	0	0
W5	-33.94	-32.06	-33.17
W6	-27.16	-23.86	-24.73
W7	-24.78	-21.84	-22.95
W8	-17.74	-14.86	-15.67
P2	-42.49	-40.87	-41.07
P3	-20.11	-15.88	-18.53
P6	-63.23	-62.72	-65.26
P8	-16.69	-13.49	-14.0
P9	-59.95	-57.95	-58.0
P10	-14.5	-12.60	-14.1
P11	-80.46	-79.65	-79.66
P12	-57.32	-56.84	-57.74
P13	-69.41	-69.09	-67.38
P14	2.50	5.13	2.19

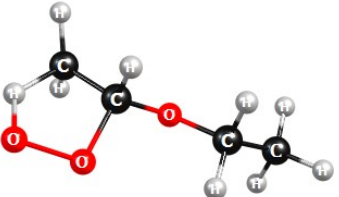
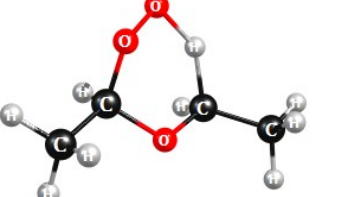
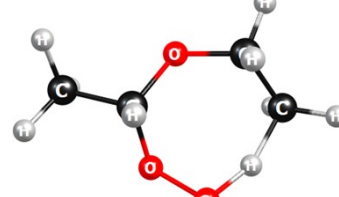
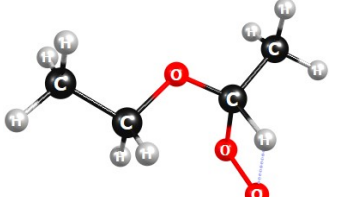
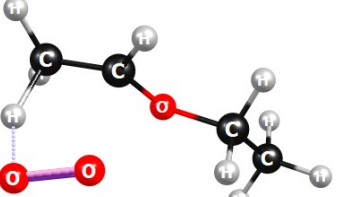
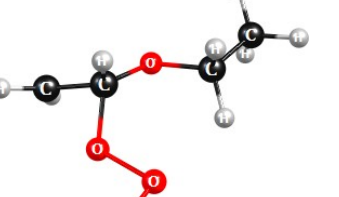
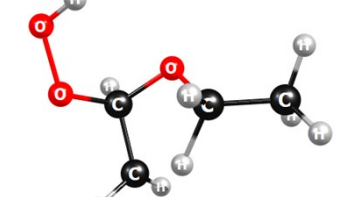
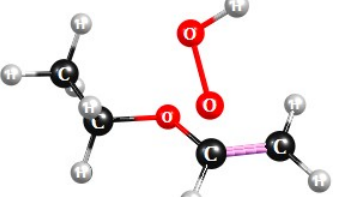
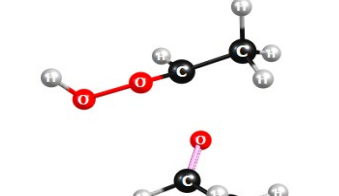
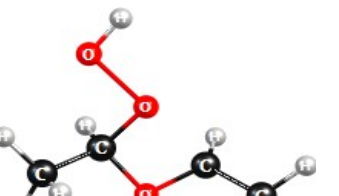
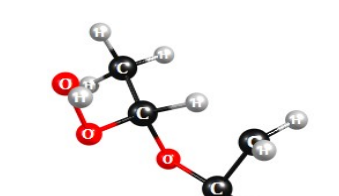
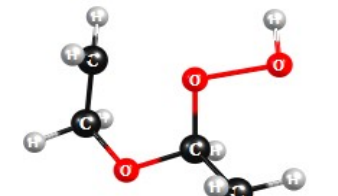
Table S6

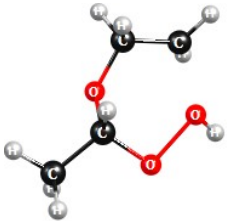
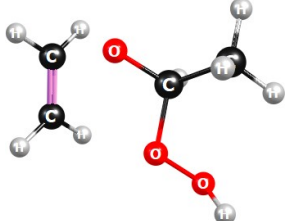
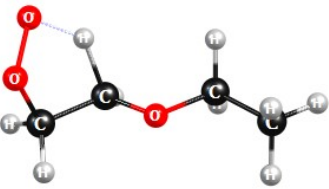
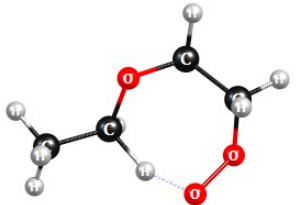
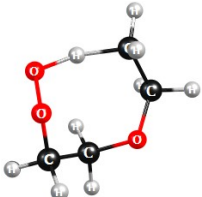
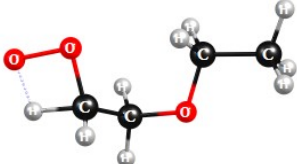
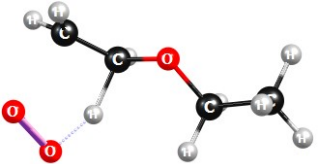
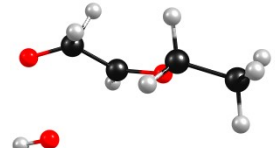
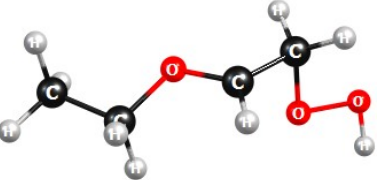
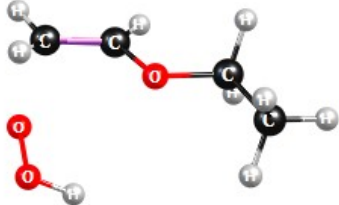
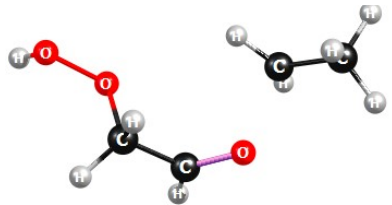
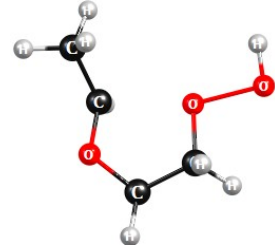
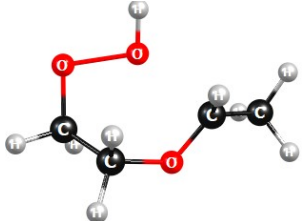
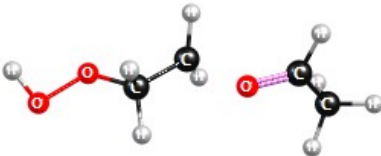
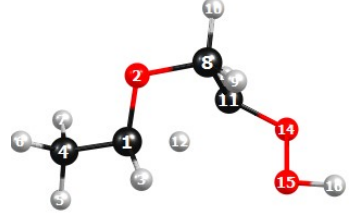
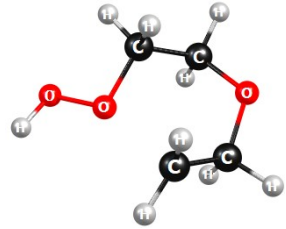
Comparison of energy barriers for reactions with transition states obtained at QCISD(T)/CBS//M06-2X/6-311++G(d,p) and M06-2X/6-311++G(d,p), in kcal mol⁻¹.

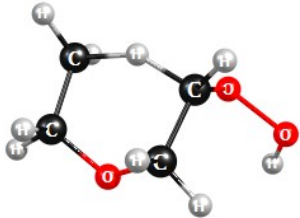
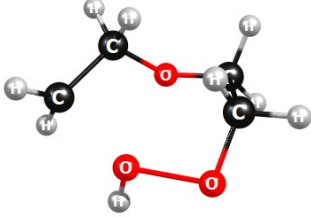
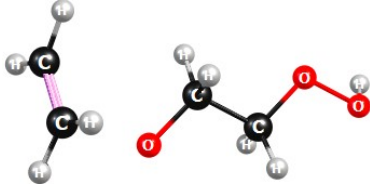
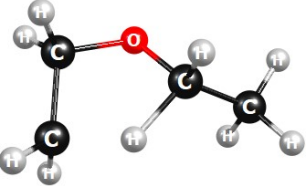
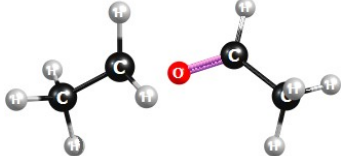
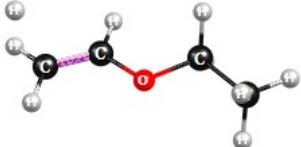
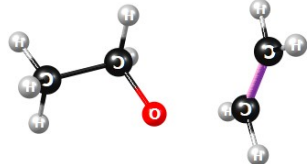
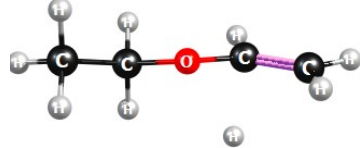
Reaction	QCISD(T)/CBS//M06-2X/6-311++G(d,p)	M06-2X/6-311++G(d,p)
W1<=>W2	36.79	39.33
W1<=>W3	18.77	20.25
W1<=>W4	24.6	24.87
W1<=>P1	38.03	40.83
W1<=>P3	28.59	30.65
W2<=>P2	10.32	14.30
W2<=>W3	16.18	16.53
W2<=>P3	15.65	16.34
W3<=>P4	15.8	20.87
W3<=>P5	18.66	22.27
W4<=>P1	15.28	18.09
W4<=>P6	12.82	15.25
W4<=>P7	17.71	20.22
W4<=>P8	23.25	24.83
W5<=>W6	26.7	30.39
W5<=>W7	18.05	18.93
W5<=>W8	24.34	24.97
W5<=>P9	41.69	45.05
W5<=>P3	31.6	34.54
W6<=>P9	19.44	21.28
W6<=>P2	10.15	13.43
W6<=>P3	15.18	16.89
W6<=>P10	25.4	27.13
W7<=>P6	9.29	12.06
W7<=>P11	13.45	15.70
W7<=>P8	22.2	23.32
W7<=>P9	23.84	24.06
W8<=>P12	13.05	15.90
W8<=>P9	15.43	15.81
W8<=>P13	17.1	19.07
W8<=>P14	24.94	27.43
R1<=>R2	26.93	28.04
R1<=>P15	23.19	24.72
R1<=>P17	38.53	39.97
R2<=>P16	24.73	27.26
R2<=>P17	33.1	34.31

Table S7

Schematic diagram of the structures of the transition states.

			
W1<=>W2	W1<=>W3	W1<=>W4	W1<=>P1
			
W1<=>P3	W2<=>P2	W2<=>W3	W2<=>P3
			
W3<=>P4	W3<=>P5	W4<=>P1	W4<=>P6

			
W4<=>P7	W4<=>P8	W5<=>W6	W5<=>W7
			
W5<=>W8	W5<=>P9	W5<=>P3	W6<=>P9
			
W6<=>P2	W6<=>P3	W6<=>P10	W7<=>P6
			
W7<=>P11	W7<=>P8	W7<=>P9	W8<=>P12

			
W8 \rightleftharpoons P9	W8 \rightleftharpoons P13	W8 \rightleftharpoons P14	R1 \rightleftharpoons R2
			
R1 \rightleftharpoons P15	R1 \rightleftharpoons P17	R2 \rightleftharpoons P16	R2 \rightleftharpoons P17

HPL rate constant for the unimolecular decomposition reaction of primary $\dot{\text{Q}}\text{OOH}$ radicals of W2 and W4 are given in Figures S2–S3. It can be seen that W2 are more inclined to decompose to cyclic ether + $\dot{\text{O}}\text{H}$. The rate constants for this channel are nearly 2 and 3 orders of magnitude faster than the C–O bond fission to P3 and H-transfer isomerization to W3, respectively. As depicted in Figure S3, there are two main competing pathways for W4 unimolecular decomposition at temperatures below 900 K, with one via 1,4 H transfer followed by rapid β -bond fission to form $\text{C}_2\text{OC}(=\text{O})\text{CH}_3 + \dot{\text{O}}\text{H}$ (P1), and the other via the cyclic ether to form $\text{CCY}(\text{COCCO}) + \dot{\text{O}}\text{H}$ (P6). The rate constants in Figure S3 (a) for these two pathways are 3 orders of magnitude faster than the others. However, as the temperature increases, the kinetic data for the channel of P11 production accelerates dramatically and becomes the primary product at temperatures above 1000 K. The reaction branching ratios depicted in Figure S3 (b) indicate that at 500 K, the formation of cyclic ethers is the dominant pathway, accounting for 60%, followed by the formation of product P1, which constitutes about 40%. As the temperature rises to 2000 K, the decomposition pathway via C–O bond fission becomes predominant, comprising 85% of the reactions. Throughout the entire temperature range, the branching ratio for the OH-transfer channel is extremely low and can be considered negligible.

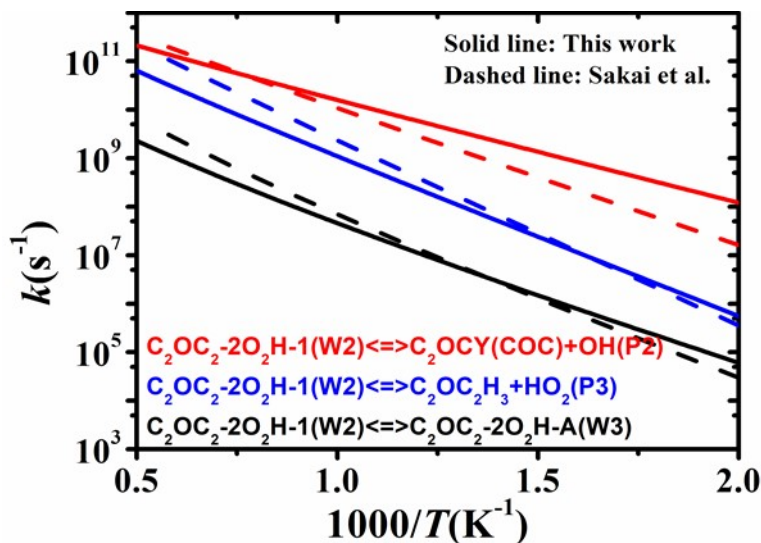


Figure. S2 HPL rate constants for the unimolecular reaction of W2. Solid line: this work, dashed line: Sakai et al [2].

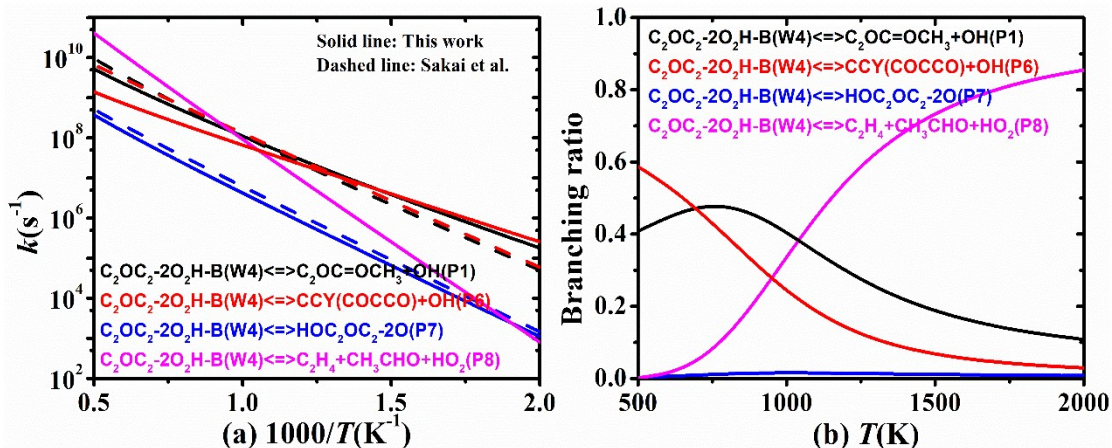


Figure. S3 HPL rate constants and branching ratios for the unimolecular reaction of W4. Solid line: this work, dashed line: Sakai et al [2].

The calculated high-pressure rate constants for the unimolecular reaction of W6 and W8, are plotted in Figure S4. With respect to the unimolecular decomposition of W6 in Figure S4 (a), the cyclic ether formation, channel P2, demonstrates the highest reactivity over the entire temperature range investigated, which is consistent with its lowest energy barrier. This is followed by the HO_2 elimination to P3 via C-O β bond fission. Channel P10 is the least reactive channel below 1000 K, while its rate constants accelerate dramatically with temperature increasing. Therefore, this channel is not negligible in the high temperature regions. As presented in Figure S4 (b), rate constants for the formation of P9 via 1,5 H-transfer is the fastest below 1000 K. When temperatures are higher than 1000 K, the C-O β -bond fission reaction channel becomes the most competitive channel.

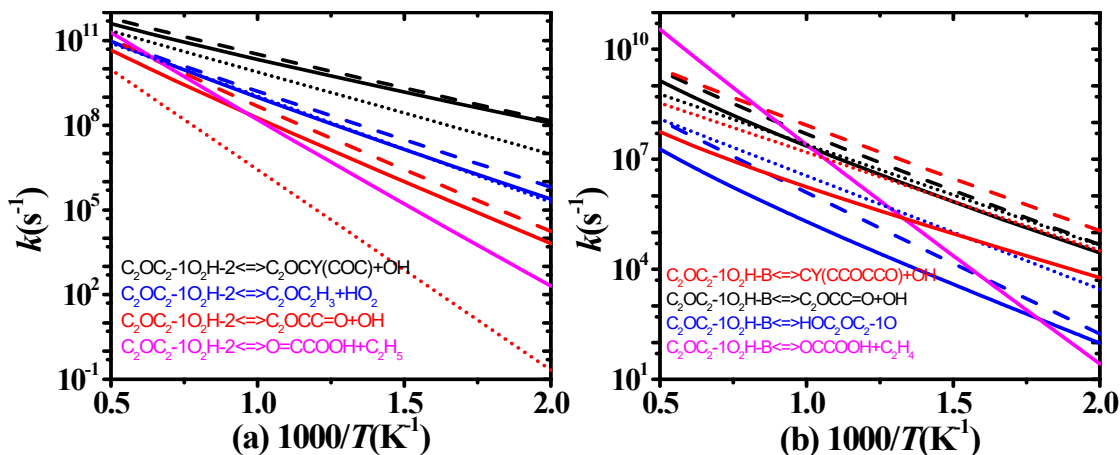


Figure S4 Calculated high-pressure limit rate constants for the unimolecular reactions of QOOH radicals: (a) $\text{C}_2\text{OC}_2-1\text{O}_2\text{H-2}$, (b) $\text{C}_2\text{OC}_2-1\text{O}_2\text{H-B}$. Solid line: this work, dashed lines : Sakai et al. [2], dotted line: Miyoshi et al. [3]

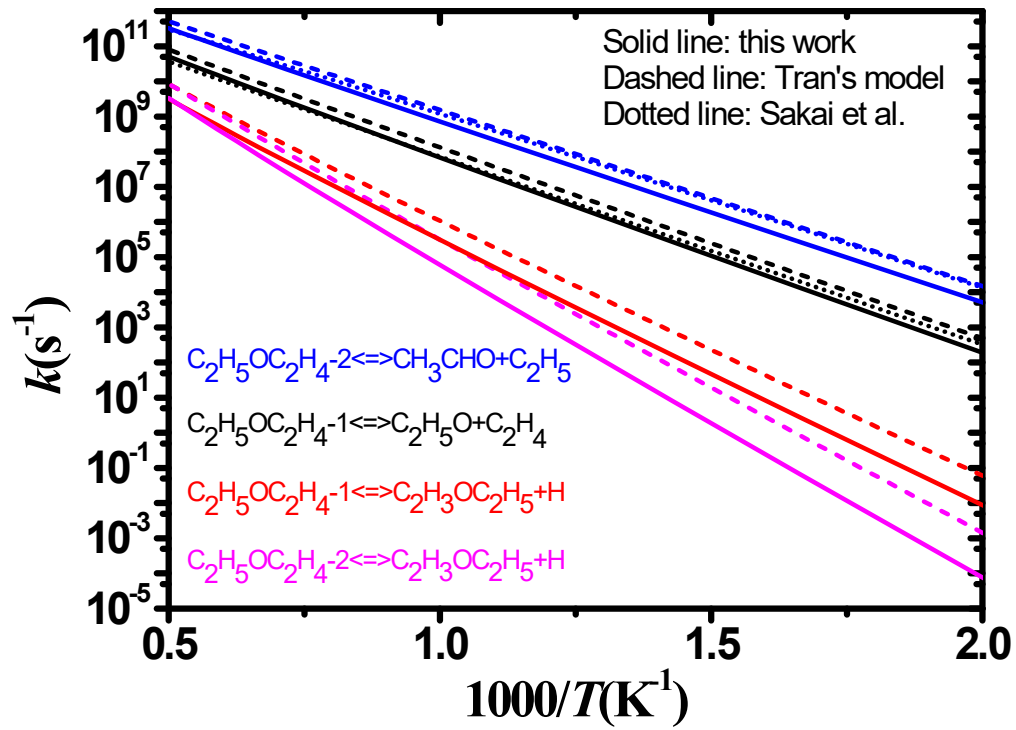


Fig. S5. Comparison of the HPL rate constants used in the kinetic model of Tran et al. [4] (dashed lines), calculated by Sakai et al. [5] (dotted lines) and our calculations (solid lines)

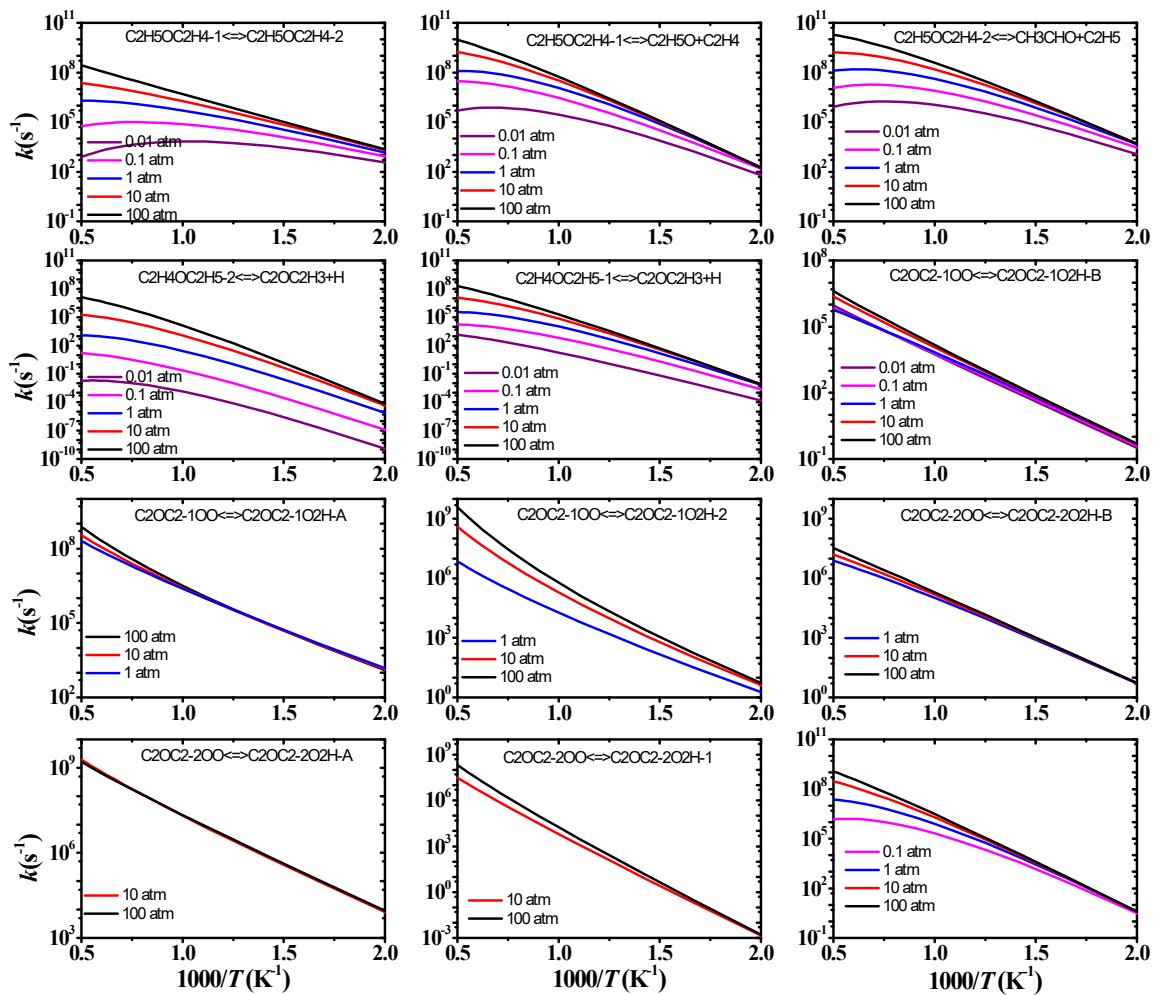


Fig. S6-1. Arrhenius plots for the reactions studied in this work.

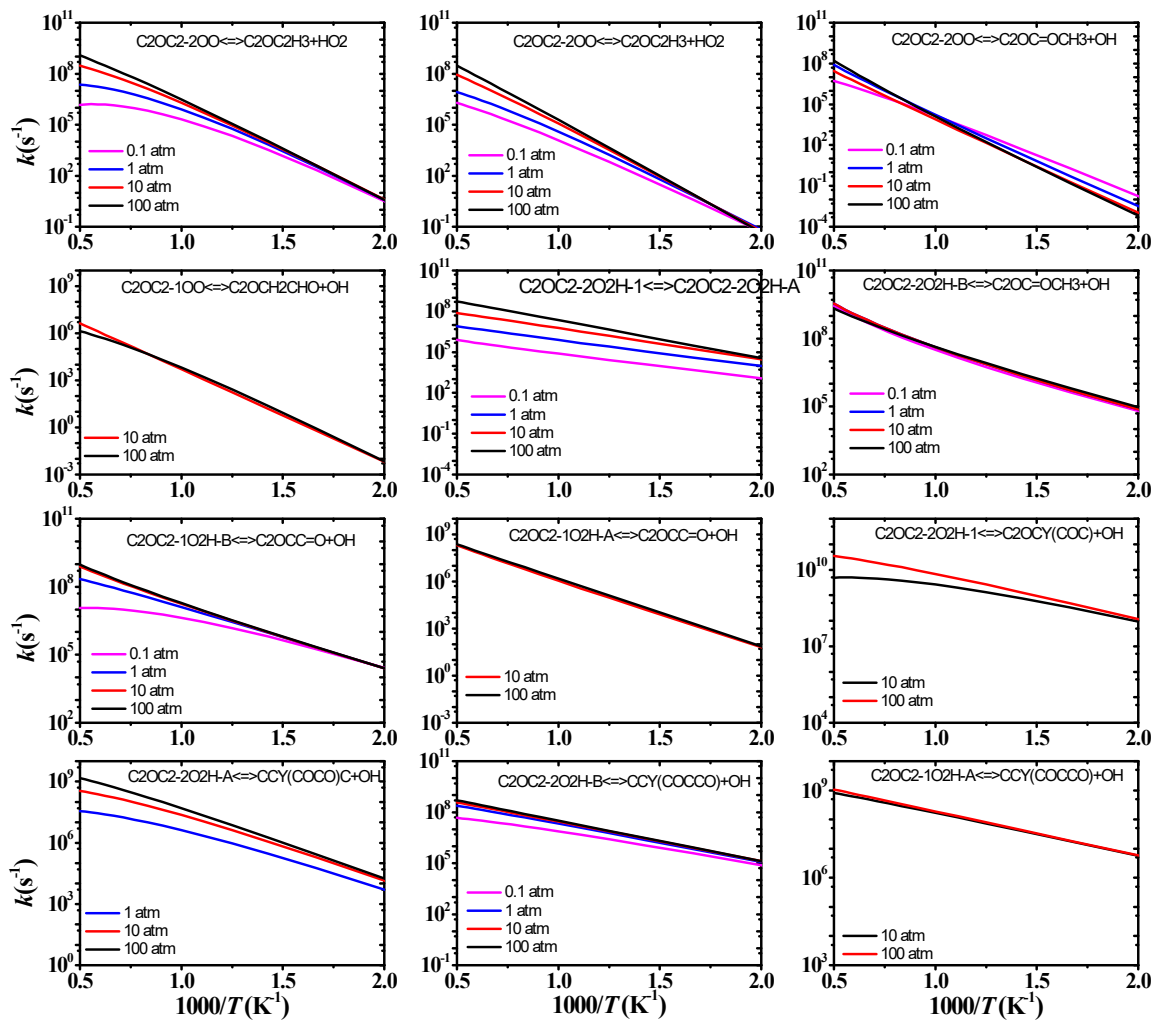


Fig. S6-2. Arrhenius plots for the reactions studied in this work.

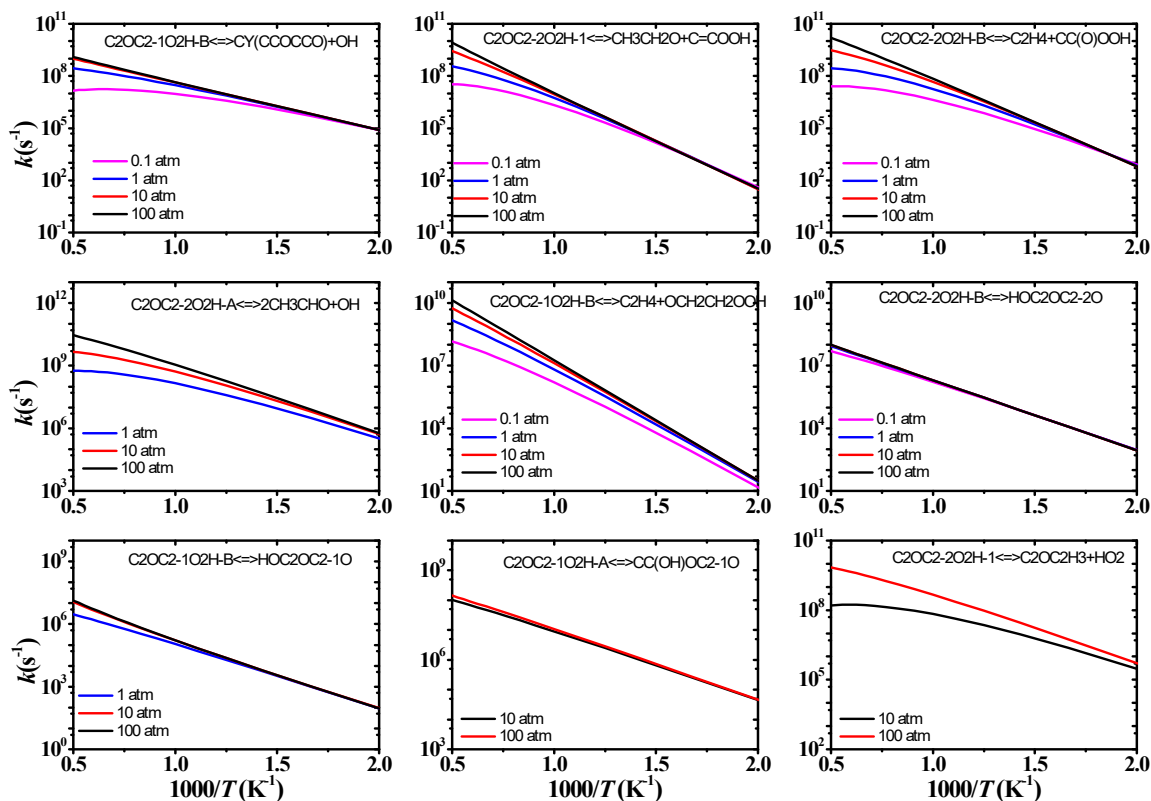


Fig. S6-3. Arrhenius plots for the reactions studied in this work.

The CBH method is for closed shell organic molecules according to the literature [6], whereas the species investigated in this work are primarily open-shell radical molecules ($\dot{\text{R}}$, $\text{R}\dot{\text{O}}_2$ and QOOH). Hence, a benchmark calculation on C_5H_6 (selected based on the literature [6]) was performed to compare the enthalpies of formation obtained via the CBH method and the atomization method with data from the existing ATcT database [7]. Furthermore, we selected one closed-shell compound $\text{CY}(\text{CCOCCO})$ from our work for CBH calculation to compare two computational methods. Two calculated species and their chemical structures are listed in Figure S7.

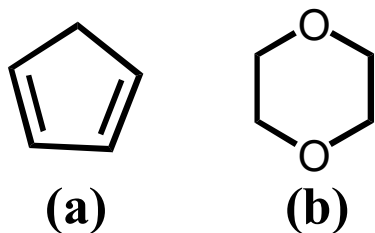


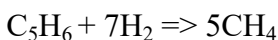
Figure S7. (a) C_5H_6 (b) $\text{CY}(\text{CCOCCO})$

Table S8. Computed enthalpies of formation (298 K, kcal/mol) using both CBH method at M06-2X/6-311++G(d,p) and atomization approach at composite methods.

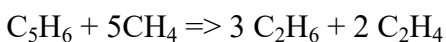
Species	CBH method			atomization approach	ATcT database ^[7]
	CBH-0	CBH-1	CBH-2		
C ₅ H ₆	-4.23	28.61	31.67	32.58	31.98
CY(CCOCCO)	-106.72	-79.25	-75.81	-77.47	-

For (a) C₅H₆:

CBH-0: based on the isogyric scheme.



CBH-1: based on the isodesmic bond separation scheme.



CBH-2: based on preserving the environment of the atoms.



According to CBH-0, reaction energy ΔH calculation:

$\Delta H = [\sum(n_i E_{\text{prod},i})] - [\sum(n_j E_{\text{react},j})]$, $E_{\text{prod}}/E_{\text{react}}$: the electronic energies at M06-2X/6-311++G(d,p) for products and reactants. Hence,

$$\Delta H = 5 E_{\text{CH}_4} - [1 E_{\text{C}_5\text{H}_6} + 7 E_{\text{H}_2}] = -85.27 \text{ kcal/mol}$$

CBH-0 standard enthalpies of formation ΔH_f of C₅H₆:

$\Delta H_{f, \text{C}_5\text{H}_6} = 5 \Delta H_{f, \text{CH}_4} - 7 \Delta H_{f, \text{H}_2} - \Delta H$, where $\Delta H_{f, \text{CH}_4} = -17.9 \text{ kcal/mol}$, $\Delta H_{f, \text{H}_2} = 0$ (from ATcT database ^[2]). Hence,

$$\Delta H_{f, \text{C}_5\text{H}_6} = -4.23 \text{ kcal/mol.}$$

According to CBH-1, reaction energy ΔH calculation:

$$\Delta H = [3 E_{\text{C}_2\text{H}_6} + 2 E_{\text{C}_2\text{H}_4}] - [1 E_{\text{C}_5\text{H}_6} + 5 E_{\text{CH}_4}] = 26.31 \text{ kcal/mol}$$

CBH-1 standard enthalpies of formation ΔH_f of C₅H₆:

$\Delta H_{f, \text{C}_5\text{H}_6} = 3 \Delta H_{f, \text{C}_2\text{H}_6} + 2 \Delta H_{f, \text{C}_2\text{H}_4} - 5 \Delta H_{f, \text{CH}_4} - \Delta H$, where $\Delta H_{f, \text{C}_2\text{H}_6} = -20.1 \text{ kcal/mol}$, $\Delta H_{f, \text{C}_2\text{H}_4} = 12.53 \text{ kcal/mol}$ (from ATcT database ^[2]). Hence,

$$\Delta H_{f, \text{C}_5\text{H}_6} = 28.61 \text{ kcal/mol.}$$

According to CBH-2, reaction energy ΔH calculation:

$$\Delta H = [E_{\text{C}_3\text{H}_8} + 4 E_{\text{C}_3\text{H}_6}] - [1 E_{\text{C}_5\text{H}_6} + 3 E_{\text{C}_2\text{H}_6} + 2 E_{\text{C}_2\text{H}_4}] = -2.50 \text{ kcal/mol}$$

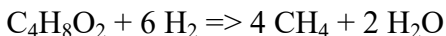
CBH-0 standard enthalpies of formation ΔH_f of C_5H_6 :

$\Delta H_{f, C_5H_6} = \Delta H_{f, C_3H_8} + 4 \Delta H_{f, C_3H_6} - 3 \Delta H_{f, C_2H_6} - 2 \Delta H_{f, C_2H_4} - \Delta H$, where $\Delta H_{f, C_3H_8} = -25.13$ kcal/mol, $\Delta H_{f, C_3H_6} = 4.77$ kcal/mol (from ATcT database [2]). Hence,

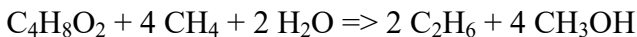
$$\Delta H_{f, C_5H_6} = 31.67 \text{ kcal/mol.}$$

For (b) CY(CCOCCO):

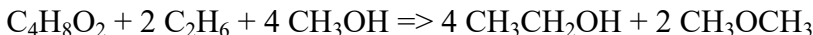
CBH-0: based on the isogyric scheme.



CBH-1: based on the isodesmic bond separation scheme.



CBH-2: based on preserving the environment of the atoms.



According to CBH-0, reaction energy ΔH calculation:

$\Delta H = [\sum(n_i E_{\text{prod},i})] - [\sum(n_j E_{\text{react},j})]$, $E_{\text{prod}}/E_{\text{react}}$: The electronic energy of products or reactants at M06-2X/6-311++G(d,p). Hence,

$$\Delta H = [4 E_{CH_4} + 2 E_{H_2O}] - [1 E_{C_4H_8O_2} + 6 E_{H_2}] = -80.56 \text{ kcal/mol}$$

CBH-0 standard enthalpies of formation ΔH_f of CY(CCOCCO):

$\Delta H_{f, CY(CCOCCO)} = 2 \Delta H_{f, H_2O} + 4 \Delta H_{f, CH_4} - 6 \Delta H_{f, H_2} - \Delta H$, where $\Delta H_{f, CH_4} = -17.9$ kcal/mol, $\Delta H_{f, H_2O} = -57.8$ kcal/mol, $\Delta H_{f, H_2} = 0$ (from ATcT database [2]). Hence,

$$\Delta H_{f, CY(CCOCCO)} = 2 \Delta H_{f, H_2O} + 4 \Delta H_{f, CH_4} - 6 \Delta H_{f, H_2} - \Delta H = -106.72 \text{ kcal/mol.}$$

According to CBH-1, reaction energy ΔH calculation:

$$\Delta H = [2 E_{C_2H_6} + 4 E_{CH_3OH}] - [1 E_{C_4H_8O_2} + 4 E_{CH_4} + 2 E_{H_2O}] = 33.84 \text{ kcal/mol}$$

CBH-1 standard enthalpies of formation ΔH_f of CY(CCOCCO):

$\Delta H_{f, CY(CCOCCO)} = 2 \Delta H_{f, C_2H_6} + 4 \Delta H_{f, CH_3OH} - 4 \Delta H_{f, CH_4} - 2 \Delta H_{f, H_2O} - \Delta H$, where $\Delta H_{f, C_2H_6} = -20.1$ kcal/mol, $\Delta H_{f, CH_3OH} = -48.1$ kcal/mol (ATcT database [2]). Hence,

$$\Delta H_{f, CY(CCOCCO)} = -79.25 \text{ kcal/mol.}$$

According to CBH-2, reaction energy ΔH calculation:

$$\Delta H = [4 E_{\text{CH}_3\text{CH}_2\text{OH}} + 2 E_{\text{CH}_3\text{OCH}_3}] - [1 E_{\text{C}_4\text{H}_8\text{O}_2} + 4 E_{\text{CH}_3\text{OH}} + 2 E_{\text{C}_2\text{H}_6}] = -4.39 \text{ kcal/mol}$$

CBH-2 standard enthalpies of formation ΔH_f of CY(CCOCCO):

$$\Delta H_{f, \text{CY(CCOCCO)}} = 4 \Delta H_{f, \text{CH}_3\text{CH}_2\text{OH}} + 2 \Delta H_{f, \text{CH}_3\text{OCH}_3} - 2 \Delta H_{f, \text{C}_2\text{H}_6} - 4 \Delta H_{f, \text{CH}_3\text{OH}} - \Delta H, \text{ where}$$

$$\Delta H_{f, \text{CH}_3\text{OCH}_3} = -44.0 \text{ kcal/mol}, \Delta H_{f, \text{CH}_3\text{CH}_2\text{OH}} = -56.2 \text{ kcal/mol (ATcT database [7])}.$$

Hence,

$$\Delta H_{f, \text{CY(CCOCCO)}} = -75.81 \text{ kcal/mol}.$$

The standard enthalpies of formation computed using both CBH method and atomization approach for C_5H_6 and CY(CCOCCO) are summarized in Table S8. It can be seen that the computed results of C_5H_6 using CBH-2 and atomization method agree well with data from ATcT database [7], with deviations of 0.31 and 0.6 kcal/mol, respectively. Moreover, compared to CBH-0 and CBH-1, the standard enthalpy of formation calculated using CBH-2 method are closer to those obtained by atomization method. The differences between CBH-2 and atomization method are 0.91 and 1.66 kcal/mol for C_5H_6 and CY(CCOCCO), respectively. However, considering computational time cost, the comparison between the two methods is limited to the two species, C_5H_6 and CY(CCOCCO).

Reference

- [1] I. Alecu, D.G. Truhlar. Computational study of the reactions of methanol with the hydroperoxyl and methyl radicals. 1. Accurate thermochemistry and barrier heights. *J. Phys. Chem. A* 115 (2011) 2811-2829.
- [2] Y. Sakai, H. Ando, H.K. Chakravarty, H. Pitsch, R.X. Fernandes. A computational study on the kinetics of unimolecular reactions of ethoxyethylperoxy radicals employing CTST and VTST. *Prod.Combust.Inst.* 35.1 (2015) 161-169.
- [3] A. Miyoshi. Systematic computational study on the unimolecular reactions of alkylperoxy (RO_2), hydroperoxyalkyl (QOOH), and hydroperoxyalkylperoxy (O_2QOOH) radicals. *J.Phys.Chem.A* 115 (2011) 3301-3325.
- [4] L.-S. Tran, O. Herbinet, Y. Li, J. Wullenkord, M. Zeng, E. Bräuer, F. Qi, K. Kohse-Höinghaus, F. Battin-Leclerc. Low-temperature gas-phase oxidation of diethyl ether: Fuel reactivity and fuel-specific products. *Proc.Combust.Inst.* 37 (2019) 511-519.
- [5] Y. Sakai, J. Herzler, M. Werler, C. Schulz, M. Fikri. A quantum chemical and kinetics modeling study on the autoignition mechanism of diethyl ether. *Proc.Combust.Inst.* 36.1 (2017) 195-202.
- [6] R.O. Ramabhadran, K. Raghavachari. Theoretical thermochemistry for organic molecules: Development of the generalized connectivity-based hierarchy. *Journal of Chemical Theory and Computation* 7 (2011) 2094-2103.
- [7] B. Ruscic, D.H. Bross. Active Thermochemical Tables: the thermophysical and thermochemical properties of methyl, CH_3 , and methylene, CH_2 , corrected for nonrigid rotor and anharmonic oscillator effects. *Molecular Physics* 119 (2021) e1969046.